Alexandria Engineering Journal (2016) 55, 2285–2297

HOSTED BY

ELSEVIER

Alexandria University

Alexandria Engineering Journal

www.elsevier.com/locate/aej
www.sciencedirect.com

ORIGINAL ARTICLE

Oberbeck–Boussinesq free convection of water based nanoliquids in a vertical channel using Dirichlet, Neumann and Robin boundary conditions on temperature

Nur Asiah Mohd Makhatar [a,c,*], **P.G. Siddheshwar** [b], **Habibis Saleh** [a], **Ishak Hashim** [a]

[a] *School of Mathematical Sciences, Universiti Kebangsaan Malaysia, 43600 UKM Bangi, Selangor, Malaysia*
[b] *Department of Mathematics, Bangalore University, Central College Campus, Bangalore 560 001, India*
[c] *Faculty of Computer and Mathematical Sciences, Universiti Teknologi MARA, 40450 Shah Alam, Selangor, Malaysia*

Received 17 November 2015; revised 5 May 2016; accepted 11 May 2016
Available online 7 June 2016

KEYWORDS

Mixed convection;
Vertical channel;
Nanoliquids;
Heat generation;
Dirichlet;
Neumann;
Robin boundary conditions

Abstract A numerical investigation is carried out into the flow and heat transfer within a fully-developed mixed convection flow of water–alumina (Al_2O_3–water), water–titania (TiO_2–water) and water–copperoxide (CuO–water) in a vertical channel by considering Dirichlet, Neumann and Robin boundary conditions. Actual values of thermophysical quantities are used in arriving at conclusions on the three nanoliquids. The Biot number influences on velocity and temperature distributions are opposite in regions close to the left wall and the right wall. Robin condition is seen to favour symmetry in the flow velocity whereas Dirichlet and Neumann conditions skew the flow distribution and push the point of maximum velocity to the right of the channel. A reversal of role is seen between them in their influence on the flow in the left-half and the right-half of the channel. This leads to related consequences in heat transport. Viscous dissipation is shown to aid flow and heat transport. The present findings reiterate the observation on heat transfer in other configurations that only low concentrations of nanoparticles facilitate enhanced heat transport for all three temperature conditions. Significant change was observed in Neumann condition, whereas the changes are too extreme in Dirichlet condition. It is found that Robin condition is the most stable condition. Further, it is also found that all three nanoliquids have enhanced heat transport compared to that by base liquid, with CuO–water nanoliquid shows higher enhancement in its Nusselt number, compared to Al_2O_3 and TiO_2.

* Corresponding author. Tel.: +60 0389213930.
E-mail address: asiah6281@gmail.com (N.A. Mohd Makhatar).

Peer review under responsibility of Faculty of Engineering, Alexandria University.

http://dx.doi.org/10.1016/j.aej.2016.05.010

Nomenclature

A	$= \frac{dP}{dX}$ constant pressure gradient
B_i	Biot numbers
L	channel width
Gr	Grashof number
Br	Brinkman number
k	thermal conductivity
C_p	specific heat at constant pressure
d_p	particle diameter
D	$= 2L$, hydraulic diameter
$\mathbf{g}$	gravitational acceleration
h	external heat transfer coefficients
Re	Reynolds number
GR	$= Gr/Re$ Mixed convection parameter defined in Eq. (18)
Nu	Nusselt number
p	pressure
P	$= p + \rho_0 \mathbf{g} X$, difference between the pressure and the hydrostatic pressure
Pr	Prandtl number
R_T	temperature ratio
S	dimensionless parameter defined in Eq. (18)
T	temperature
u	dimensionless velocity in the y direction
U	velocity components in the Y-direction
X, Y	dimensionless space coordinates

Greek symbols

α	$= k/(\rho_0 c_p)$, thermal diffusivity
β	thermal expansion coefficient
θ	dimensionless temperature
ν	kinematic viscosity
μ	dynamic viscosity
ρ	density
ϕ	volume fraction of nanoparticles.

Subscripts

0	value on channel entrance
1	left wall
2	right wall
bl	base liquid
nl	nanoliquid
np	nanoparticles

1. Introduction

The vertical channel is a commonly used configuration in many thermal engineering equipments. Some application areas involving the configuration are collector of solar energy, cooling devices of electronic and micro-electronic equipments, packed chemical reactors, prevention of subsoil water pollution, geothermal reservoirs, nuclear waste disposal and cooling of nuclear reactors. Some important reported works on the problem include those of Tao [31], Aung and Worku [2], Incropera [17], Cheng et al. [9], Javeri [18], Barletta [4], Zanchini [35], Barletta and Zanchini [5], Grosan and Pop [15], Pop et al. [26] and Saleh et al. [29]. Except Javeri [18] and Zanchini [35], all others considered Dirichlet boundary condition on temperature.

Viscous dissipation aids flow in the case of both upward flow and downward flow. It is also observed that small value of pertubation parameter is agreed very well in analytical and numerical solutions. Chao et al. [8] later investigated numerically the heat transfer and entropy generation within a fully-developed flow of water-based nanoliquid in a vertical channel. They provide a useful insight into the effects of viscous dissipation on the entropy generation within vertical asymmetrically-heated channels containing mixed convection flow. Meanwhile, the study by Barletta [4] shows that especially in the case of upward flow, the effects of viscous dissipation can be important. It was also concluded that viscous dissipation enhances the effect of flow reversal for downward flow.

Three types of boundary conditions are compared in this study, comprising the Dirichlet (first kind), Newmann (second kind) and Robin (third kind). In Dirichlet condition, the value is set of the unknown function itself, whereas in Newmann condition the gradient of the function is set in a direction normal to the boundary. The Robin condition sets the value of a combination of the unknown function and its normal gradient that is linear in the unknown function. Among the earlier systematic comparisons of the effect of these boundary conditions were by Novy et al. [23], Bixler [6] and Papanastasiou et al. [24]. It was proven that the Robin boundary condition gives the most accurate solution. Hence, the Robin condition is applied for the default case in this study.

It was Choi and Eastman [10] who gave the name nanoliquids to liquids with suspended nanoparticles. Ever since the manufacture of nanoparticles became a reality, researcher started using nanoliquids as a preferred medium for heat transfer. Investigations have been done on mixed convective flows of nanoliquids in channels by many researchers and include Xu et al. [33], where it was found that the heat transfer characteristic can be improved significantly as the proper nanoliquids are applied. Mahian et al. [20] revealed that $Ti0_2$–water nanoliquids reduces the entropy generation in the vertical channel. Other related studies are by Xu and Pop [34], Hajipour and Dehkordi [16], Chao et al. [8], Farooq et al. [13], Fakour et al. [12], Das et al. [11] and Malvandi and Ganji [22]. These works, use either the single-phase model of Khanafer et al. [19] or the Buongiorno [7] model and their investigations are based on the Dirichlet condition on temperature with mostly no viscous dissipation effect. It is now known in nanoliquids based applications that the 'enhanced heat transfer' situation is seen only for dilute concentration of nanoparticles. With this being the case, there is ample opportunity in the nanoliquids to have viscous dissipation and hence is an important aspect to investigate in vertical channel flows. The objective in the present work was the following:

1. To consider the effect of Robin temperature boundary condition on the flow and heat transfer in three water-based nanoliquids.

2. To ascertain whether viscous dissipation plays its classical role on flow and heat transfer in the three chosen nanoliquids.
3. To consider various volume fractions of nanoparticles and see whether enhanced heat transfer situation persists in dilute nanoliquids when a Robin condition is used.
4. To make a comparison between the extent of heat transfers facilitated by the Dirichlet, Neumann and Robin boundary conditions.
5. To verify the hypothesis that all three nanoliquids transfer more heat compared to base liquid water for all three boundary conditions.

There are various types of analytical or numerical methods which can be employed to solve the nonlinear systems of ordinary differential equations. Among others are done by Rashidi et al. [27], where a combination of the differential transform method (DTM) and Pad approximation method was applied. Meanwhile, Freidoonimehr et al. [14] applied the fourth order Runge–Kutta method based shooting technique and Abolbashari et al. [1] use Optimal Homotopy Analysis Method (OHAM). Later, Rashidi et al. [28] applied fourth order RungeKutta method. For this study, though the governing equations seem simple, clearly they are not analytically tractable due to the use of a more realistic Robin boundary condition on temperature. Hence, shooting method is used to solve for the flow and temperature distributions.

2. Mathematical formulation and validation

Mixed convection flow of three water-based nanoliquids with copper, alumina or titania nanoparticles is investigated in this study. We consider under the Boussinesq–Oberbeck approximation, the steady flow of a Newtonian fluid in a parallel plate vertical channel of width L. The x-axis is chosen to be vertically upwards opposite in direction to the gravitational vector $\mathbf{g}$. The y-axis is perpendicular to the channel walls and the origin of the axes is on the left channel wall. The flow has a uniform upward vertical velocity U_0, at the channel entrance. The physical configuration is as shown in Fig. 1. The thermophysical properties of the nanoliquid except density are assumed to be constant. The Oberbeck–Boussinesq approximation is used and the equation of state under this assumption is

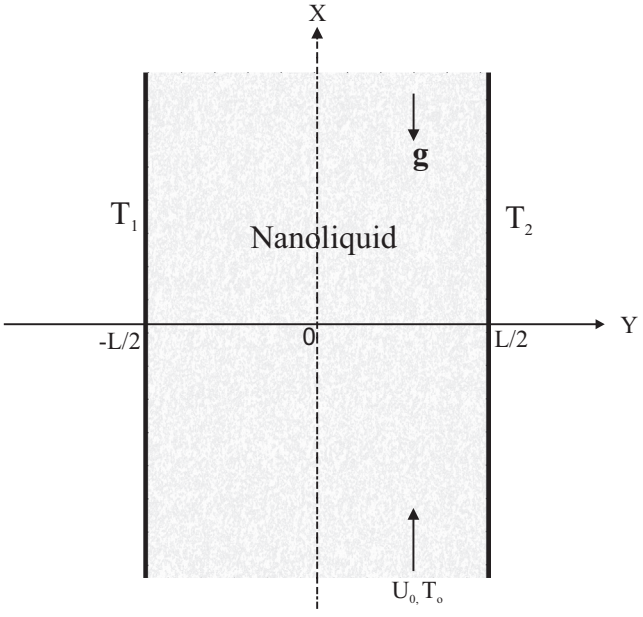

Figure 1 Physical configuration of vertical channel containing fully-developed mixed convection nanoliquid flow.

$$\rho_{nl} = \rho_{0_{nl}}[1 - \beta_{nl}(T - T_0)]. \tag{1}$$

The X-component U is the only nonzero component of the velocity. Thus, the continuity equation is

$$\frac{dU}{dY} = 0. \tag{2}$$

The momentum balance equations along X and Y directions are modified for nanoliquids using Khanafer et al. [19] model to obtain:

$$(\rho\beta)_{nl}\mathbf{g}(T - T_0) + \mu_{nl}\frac{\mathrm{d}^2U}{\mathrm{d}Y^2} - \frac{\partial P}{\partial X} = 0, \tag{3}$$

$$\frac{\partial P}{\partial Y} = 0, \tag{4}$$

where μ_{nl} is the effective dynamic viscosity of the nanoliquid, applying the correlation model by Azmi et al. [3]:

$$\mu_{nl} = \mu_{bl}(1 + \phi)^{11.3}\left(1 + \frac{T}{70}\right)^{-0.038}\left(1 + \frac{d_p}{170}\right)^{-0.061}. \tag{5}$$

Meanwhile, ρ_{nl} is the effective density of the nanoliquid and β_{nl} is the effective thermal expansion coefficient of the nanoliquid. They are given by the following expressions from mixture theory:

$$\begin{aligned}\rho_{nl} &= (1 - \phi)\rho_{bl} + \phi\rho_{np},\\ (\rho\beta)_{nl} &= (1 - \phi)(\rho\beta)_{bl} + \phi(\rho\beta)_{np}.\end{aligned} \tag{6}$$

where $P = p + \rho_0\mathbf{g}X$. In view of Eqs. (4), (3) can be rewritten as

$$T - T_0 = \frac{1}{(\rho\beta)_{nl}\mathbf{g}}\frac{\mathrm{d}P}{\mathrm{d}X} - \frac{\mu_{nl}}{(\rho\beta)_{nl}\mathbf{g}}\frac{\mathrm{d}^2U}{\mathrm{d}Y^2}. \tag{7}$$

The boundary conditions on U are taken as follows:

$$U\left(-\frac{L}{2}\right) = U\left(\frac{L}{2}\right) = 0. \tag{8}$$

Differentiating Eq. (7) with respect to X and then separately with respect to Y, we get

$$\frac{\partial T}{\partial X} = \frac{1}{(\rho\beta)_{nl}\mathbf{g}}\frac{\mathrm{d}^2P}{\mathrm{d}X^2}, \tag{9}$$

$$\frac{\partial T}{\partial Y} = -\frac{\mu_{nl}}{(\rho\beta)_{nl}\mathbf{g}}\frac{\mathrm{d}^3U}{\mathrm{d}Y^3}. \tag{10}$$

The boundary conditions on the temperature field are assumed to be the following:

$$-k_{nl}\left.\frac{\partial T}{\partial Y}\right|_{Y=-\frac{L}{2}} = h_1[T_1 - T(X, -L/2)], \tag{11}$$

$$-k_{nl}\left.\frac{\partial T}{\partial Y}\right|_{Y=\frac{L}{2}} = h_2[T(X, L/2) - T_2], \tag{12}$$

where h_1 and h_2 are constants.Using Eq. (10), Eqs. (11) and (12) are rewritten as

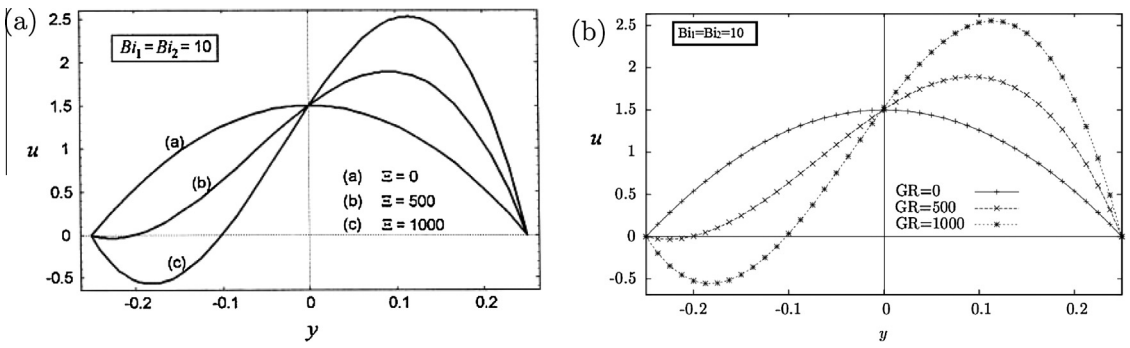

Figure 2 Velocity profiles of (a) Zanchini [35] and (b) present study for different Mixed convection parameter GR with $Br = 0, Bi_1 = Bi_2 = 10$ and $\phi = 0$.

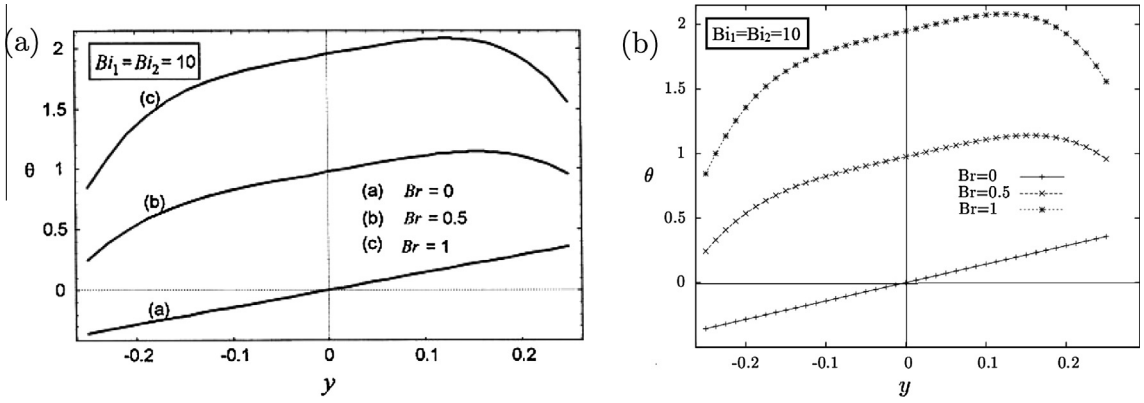

Figure 3 Temperature profiles of (a) Zanchini [35] and (b) present study for different Brinkman number Br with $GR = 0, Bi_1 = Bi_2 = 10$ and $\phi = 0$.

Table 1 Thermophysical properties of water at 300 K.

ρ_{bl}	$(C_p)_{bl}$	$(\rho C_p)_{bl}$	k_{bl}	β_{bl}	$(\rho\beta)_{bl}$	μ_{bl}
997.1	4179	4.1669E5	0.6	2.1E−4	2.09E−1	8.91E−4

$$\left.\frac{\mathrm{d}^3U}{\mathrm{d}Y^3}\right|_{Y=-\frac{L}{2}} = \frac{(\rho\beta)_{nl}\mathbf{g}h_1}{k_{nl}\mu_{nl}}[T_1 - T(X,-L/2)], \tag{13}$$

$$\left.\frac{\mathrm{d}^3U}{\mathrm{d}Y^3}\right|_{Y=\frac{L}{2}} = \frac{(\rho\beta)_{nl}\mathbf{g}h_2}{k_{nl}\mu_{nl}}[T(X,L/2) - T_2]. \tag{14}$$

It is easily verified that Eqs. (13) and (14) imply that $\partial T/\partial X$ is zero both at $Y = -L/2$ and at $Y = L/2$. Since Eq. (9) ensures that $\partial T/\partial X$ does not depend on Y, it is concluded that $\partial T/\partial X$ is zero everywhere. Therefore, the temperature T depends only on Y, i.e., $T = T(Y)$. Thus, on account of Eq. (9), we may write

$$\frac{\mathrm{d}P}{\mathrm{d}X} = A. \tag{15}$$

The conservation of energy equation in the presence of viscous dissipation is taken to be the following:

$$k_{nl}\frac{\mathrm{d}^2T}{\mathrm{d}Y^2} = -\mu_{nl}\left(\frac{\mathrm{d}U}{\mathrm{d}Y}\right)^2. \tag{16}$$

The expression for k_{nl} is taken from the relation of Patel's model, Patel et al. [25]:

$$k_{nl} = k_{bl}\left(1 + 0.135\left(\frac{k_{np}}{k_{bl}}\right)^{0.273}\left(\frac{T}{20}\right)^{0.547}\left(\frac{100}{d_p}\right)^{0.234}\phi^{0.467}\right). \tag{17}$$

The expression for μ_{nl} is as mentioned earlier in Eq. (5). We now define $D = 2L$ which is the hydraulic diameter and the reference velocity U_0 and the reference temperature T_0 are given by

Table 2 Thermophysical properties of nanoparticles at 300 K.

Nanoparticle	ρ_{np}	$(C_p)_{np}$	$(\rho C_p)_{np}$	k_{np}	β_{np}	$(\rho\beta)_{np}$
CuO	8954	383	3.429E6	400	1.67E−5	1.495E−1
Al_2O_3	3600	765	2.754E6	46	0.63E−5	2.268E−2
TiO_2	4250	686.2	2.916E6	8.954	0.9E−5	3.825E−2

Table 3 Effective values of properties of nanoparticles–water at 300 K, $d_p = 50$.

	ϕ	$(\rho C_p)_{\mathrm{nl}}$	k_{nl}	$(\rho\beta)_{\mathrm{nl}}$	μ_{nl}	$\frac{(\rho\beta)_{\mathrm{nl}}}{(\rho\beta)_{\mathrm{bl}}}$	$\frac{\mu_{\mathrm{nl}}}{\mu_{\mathrm{bl}}}$	$\frac{k_{\mathrm{nl}}}{k_{\mathrm{bl}}}$
CuO–water	0.005	4.163E6	0.6090	0.2091	0.915E−3	0.999	1.027	1.101
	0.010	4.160E6	0.6181	0.2090	0.969E−3	0.997	1.087	1.134
	0.015	4.156E6	0.6273	0.2085	1.024E−3	0.996	1.149	1.167
	0.020	4.152E6	0.6366	0.2082	1.083E−3	0.994	1.215	1.193
	0.025	4.148E6	0.6459	0.2079	1.144E−3	0.993	1.284	1.214
	0.030	4.145E6	0.6554	0.2076	1.208E−3	0.991	1.356	1.233
Al_2O_3–water	0.005	4.160E6	0.6087	0.2085	0.915E−3	0.956	1.027	1.056
	0.010	4.153E6	0.6175	0.2075	0.969E−3	0.991	1.087	1.077
	0.015	4.146E6	0.6264	0.2070	1.024E−3	0.987	1.149	1.093
	0.020	4.139E6	0.6353	0.2057	1.083E−3	0.982	1.215	1.107
	0.025	4.132E6	0.6444	0.2047	1.144E−3	0.978	1.284	1.119
	0.030	4.124E6	0.6535	0.2038	1.208E−3	0.973	1.356	1.129
TiO_2–water	0.005	4.161E6	0.6074	0.2085	9.15E−3	0.9969	1.027	1.036
	0.010	4.154E6	0.6149	0.2077	0.969E−3	0.992	1.087	1.049
	0.015	4.148E6	0.6225	0.2068	1.024E−3	0.988	1.149	1.060
	0.020	4.142E6	0.6301	0.2060	1.083E−3	0.984	1.215	1.068
	0.025	4.136E6	0.6348	0.2051	1.144E−3	0.980	1.284	1.076
	0.030	4.130E6	0.6456	0.2043	1.208E−3	0.975	1.356	1.083

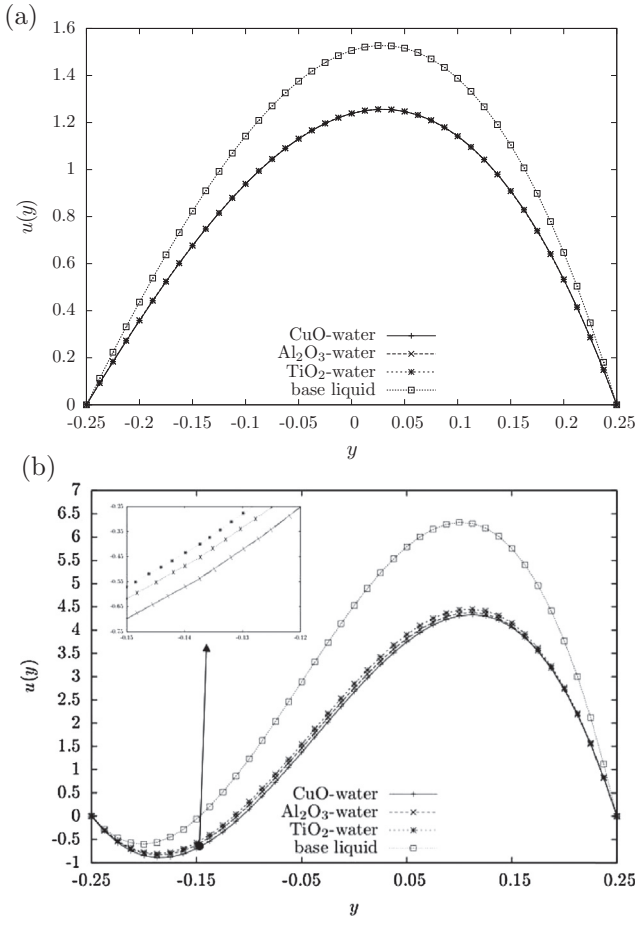

Figure 4 Velocity profiles of three types of water-based nanoliquids and base liquid for two various values of GR, (a) $GR = 100$ and (b) $GR = 800$ with $Br = 0.001, Bi_1 = Bi_2 = 10$ and $\phi = 0.02$.

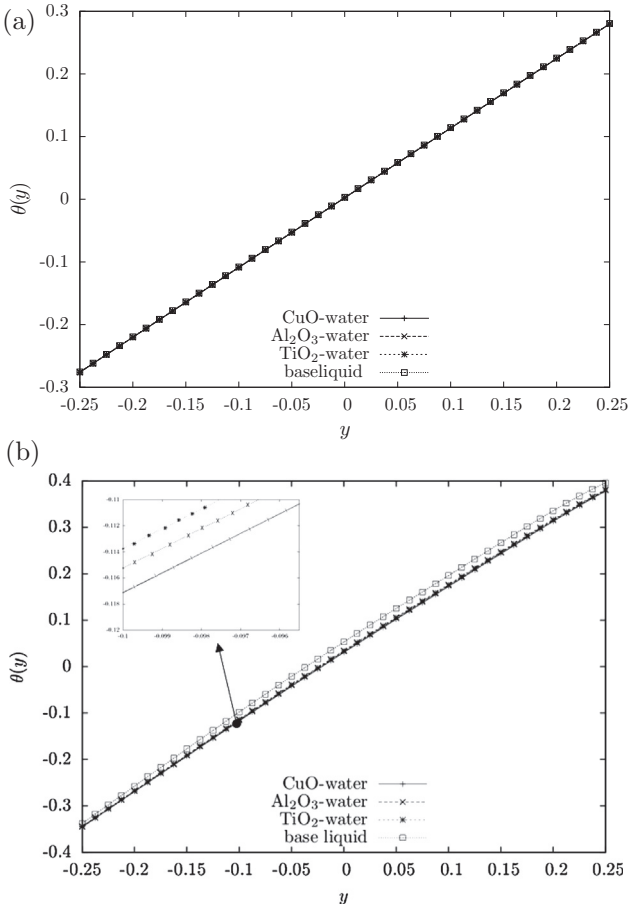

Figure 5 Temperature profiles of three types of water-based nanoliquids and base liquid for two various values of GR, (a) $GR = 100$ and (b) $GR = 800$ with $Br = 0.001, Bi_1 = Bi_2 = 10$ and $\phi = 0.02$.

$$U_0 = -\frac{AD^2}{48\mu_{\rm bl}},$$
$$T_0 = \frac{T_1+T_2}{2} + S\left(\frac{1}{Bi_1}-\frac{1}{Bi_2}\right)(T_2-T_1), \tag{18}$$
$$\text{where} \quad Bi_1 = \frac{h_1 D}{k_{\rm bl}} \quad \text{and} \quad Bi_2 = \frac{h_2 D}{k_{\rm bl}}.$$

Eqs. (7), (8), (11), (12) and (16) can be written in a dimensionless form by employing the following dimensionless parameters:

$$u = \frac{U}{U_0}, \qquad \theta = \frac{T-T_0}{T_2-T_1}, \qquad y = \frac{Y}{D}, \qquad Gr = \frac{\mathbf{g}\beta_{\rm bl}\Delta T D^3}{(\nu_{\rm bl})^2},$$
$$Br = \frac{\mu_{\rm bl}(U_0)^2}{k_{\rm bl}\Delta T}, \qquad Pr = \frac{\nu_{\rm bl}}{\alpha_{\rm bl}}, \qquad GR = \frac{Gr}{Re}, \qquad R_T = \frac{T_2-T_1}{\Delta T},$$
$$Re = \frac{U_0 D}{\nu_{\rm bl}}, \qquad S = \frac{Bi_1 Bi_2}{Bi_1 Bi_2 + 2Bi_1 + 2Bi_2}. \tag{19}$$

The non-dimensional governing equations and boundary conditions are as follows:

$$\frac{\mu_{\rm nl}}{\mu_{\rm bl}}\frac{{\rm d}^2u}{{\rm d}y^2} = -\left[48 + \frac{(\rho\beta)_{\rm nl}}{(\rho\beta)_{\rm bl}} GR\theta\right], \tag{20}$$
$$u(-1/4) = u(1/4) = 0, \tag{21}$$
$$\frac{1}{Br}\left(\frac{k_{\rm nl}}{k_{\rm bl}}\right)\frac{{\rm d}^2\theta}{{\rm d}y^2} + \left(\frac{\mu_{\rm nl}}{\mu_{\rm bl}}\right)\left(\frac{{\rm d}u}{{\rm d}y}\right)^2 = 0, \tag{22}$$
$$\left.\frac{{\rm d}\theta}{{\rm d}y}\right|_{y=-\frac{1}{4}} = Bi_1\left[\theta\left(-\frac{1}{4}\right) + \frac{R_T S}{2}\left(1+\frac{4}{Bi_1}\right)\right], \tag{23}$$
$$\left.\frac{{\rm d}\theta}{{\rm d}y}\right|_{y=\frac{1}{4}} = Bi_2\left[-\theta\left(\frac{1}{4}\right) + \frac{R_T S}{2}\left(1+\frac{4}{Bi_2}\right)\right]. \tag{24}$$

The dimensionless form of velocity and temperature profiles thus depends on five parameters: the ratio $GR = Gr/Re$, the Brinkman number Br, the temperature difference ratio R_T and the Biot numbers Bi_1 and Bi_2. Following the work of Zanchini [35], the Nusselt numbers calculated at the left and right vertical plates are given by the following:

$$Nu_1 = \frac{\left(\frac{k_{\rm nl}}{k_{\rm bl}}\right)}{R_T[\theta(1/4)-\theta(-1/4)] + (1-R_T)}\left.\frac{{\rm d}\theta}{{\rm d}y}\right|_{y=-1/4},$$
$$Nu_2 = \frac{\left(\frac{k_{\rm nl}}{k_{\rm bl}}\right)}{R_T[\theta(1/4)-\theta(-1/4)] + (1-R_T)}\left.\frac{{\rm d}\theta}{{\rm d}y}\right|_{y=1/4}. \tag{25}$$

Eqs. (20) and (22) on eliminating temperature yield a 4th order nonlinear ordinary differential equation in U but need two additional boundary conditions on U to be generated. This was impossible to do in view of third type boundary condition on θ. Hence, the coupled system of Eqs. (20) and (22) subject to conditions (21) (23) and (24) is solved by Runge–Kutta method with shooting technique.

In order to validate the numerical code, it is necessary to make a comparison with the previous published results. The present numerical results are verified against the result obtained by Zanchini [35] as shown in Figs. 2 and 3 for $\phi = 0$. Clearly, from this comparison, the present results are in excellent agreement with the corresponding results by Zanchini [35].

3. Results and discussions

The study involves fully developed mixed convection flow in a nanoliquid, focusing on the effects of nanoliquid properties, the Brinkman number, the mixed convection parameter, Biot number and the Nusselt number. The value of temperature ratio R_T, the particle diameter d_p(nm) and the temperature T ($^\circ C$) are kept at 1, 50 and 30 respectively. Meanwhile, the effect of nanoparticle volume fraction is investigated in the range of $0.005 \leqslant \phi \leq 0.3$. The default values of other parameters are mentioned in the description of the respective figures. The built-in routine, *dsolve* (in Maple), is applied for the numerical computations. Tables 1–3 respectively represent the values of the quantities of base liquid, nanoparticles and effective values of quantities concerning the nanoliquids. For the investigations, three water-based nanoliquids with copperoxide, alumina and titania nanoparticles are considered. From these tables, it is obvious that the magnitude of quantities of nanoliquids is in between those of nanoparticles and base liquid. Table 3 gives us the information on the ratio of nanoliquid values and the base liquid values for kinematic viscosity (ν), dynamic viscosity (μ) and the effect thermal expansion ($\rho\beta$).

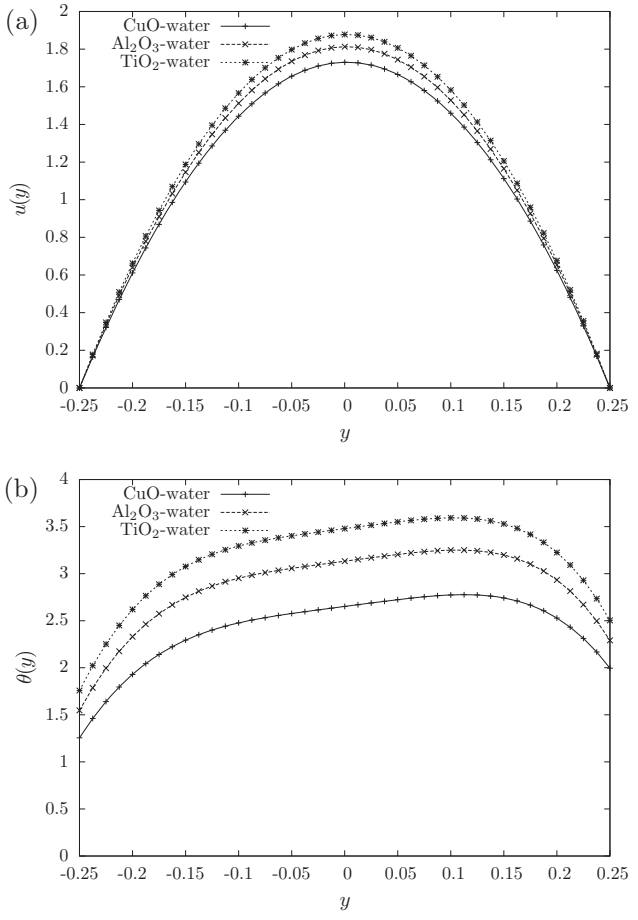

Figure 6 (a) Velocity profile and (b) temperature profile of three types of water-based nanoliquids with low mixed convection parameter $GR = 10$, high Brinkman number $Br = 1.0, Bi_1 = Bi_2 = 10$ and $\phi = 0.02$.

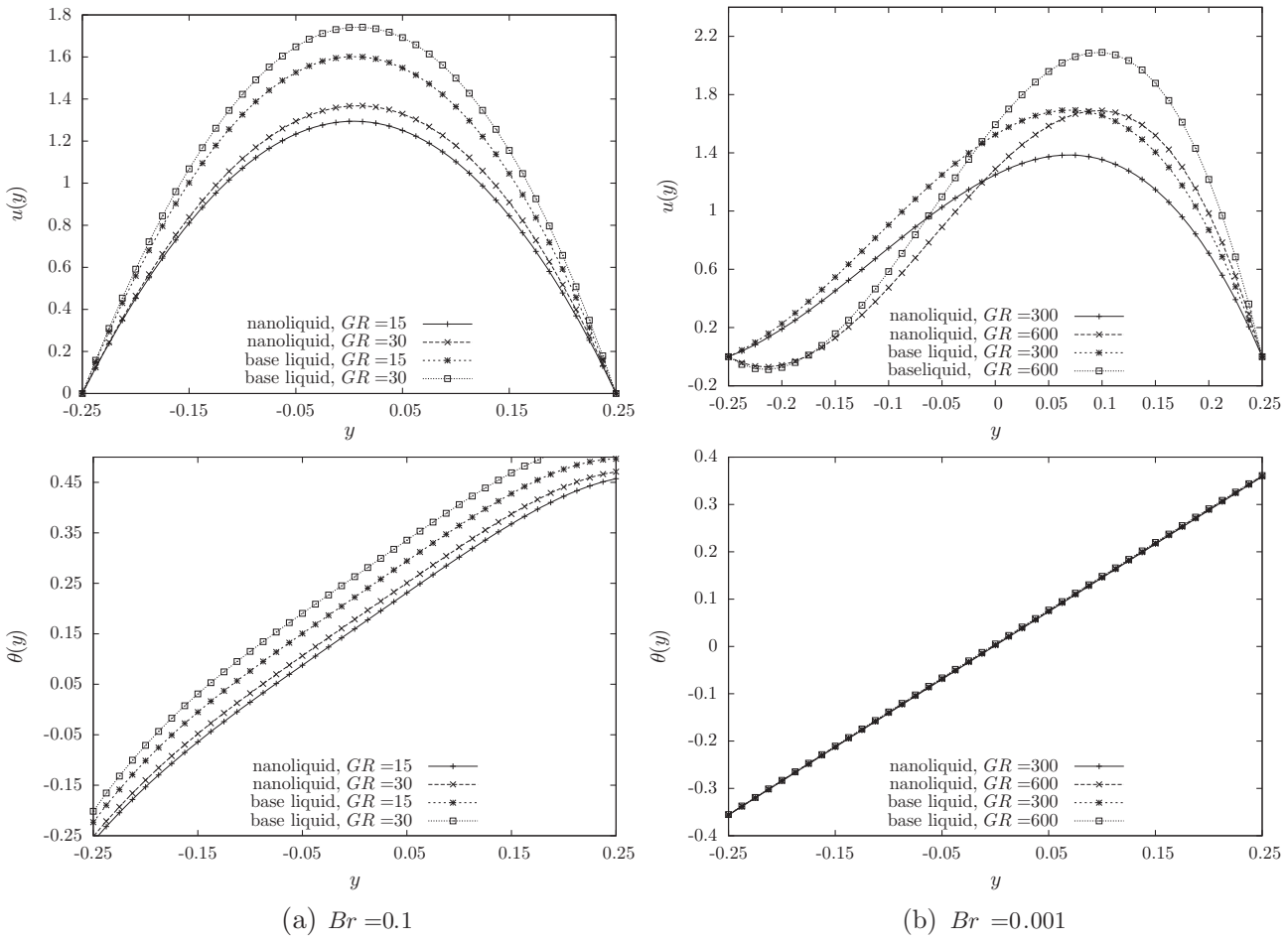

Figure 7 Velocity profiles and temperature profiles of nanoliquid (using Al_2O_3–water, $\phi = 0.02$) and base liquid with $Bi_1 = Bi_2 = 10$. Fig. 4(a): High value of Brinkman number $Br = 0.1$ and low values of mixed convection parameter GR. Fig.4(b): Low value of Brinkman number $Br = 0.001$ and high values of mixed convection parameter GR.

These ratio values for the respective nanoliquids at six different values of ϕ are applied in solving Eqs. (20) and (22).

3.1. Velocity and temperature profiles

Figs. 4 and 5 represent the velocity and the temperature profiles respectively for base liquid and three kinds of water-based nanoliquids with the mixed convection parameter values, $GR = 100$ and $GR = 800$ and constant values of Brinkman number $Br = 0.001$, Biot numbers $Bi_1 = 10, Bi_2 = 10$ and nanoparticles volume fraction $\phi = 0.02$. In Fig. 4(a), the velocity for all the three water-based nanoliquids does not show any significant difference and uniform when $GR = 100$. Meanwhile, looking into Fig. 4(b), the increase in GR increases the buoyancy force and subsequently the liquid velocity in the flow direction. This is because natural and forced convection effects are shown by GR, having the flow dominated by the natural convection and buoyancy force. Furthermore, high additive content in TiO_2–water leads to a high buoyancy force. Hence, with the increase in GR, the velocity magnitude of TiO_2–water is highest, followed by Al_2O_3–water and CuO–water throughout the channel. On top of that, with a high value of GR, reflow phenomenon occurs for the water-based nanoliquids and the base liquid. As the liquid made contact with the colder wall, it shrinks accordingly. With this, reverse flow occurs due to the increase in density and the reduction of buoyancy force in the upward direction. Meanwhile, looking at the temperature profiles in Fig. 5, the temperature values when $GR = 800$ is slightly higher than that when $GR = 100$, for the case of all the nanoliquids and more obvious for the case of base liquid. The reason being is based on what was observed in the velocity profiles, where a more intense mixed convection results in a larger temperature gradient, leading to a greater buoyancy force. The equivalent thermal expansion coefficient for nanoliquids is less than base liquid although the nanoliquids are more dense, while its viscosity is higher. As a result, lower gravitational force gives less affects in the reflow region and hence, its velocity is more uniformly distributed and lower than the base liquid.

As discussed in Utomo et al. [32], the relative viscosity of TiO_2–water is higher than Al_2O_3–water and CuO–water. This is due to higher additive content in TiO_2–water. The additives (surfactants and/or organic polymers) used to stabilise nanoliquid may lower the effective thermal conductivity of base liquid since they usually have lower thermal conductivity than water. They can also form a "skin" around nanoparticles and introduce contact resistance to heat conduction. This could clearly be seen in the velocity profile and temperature

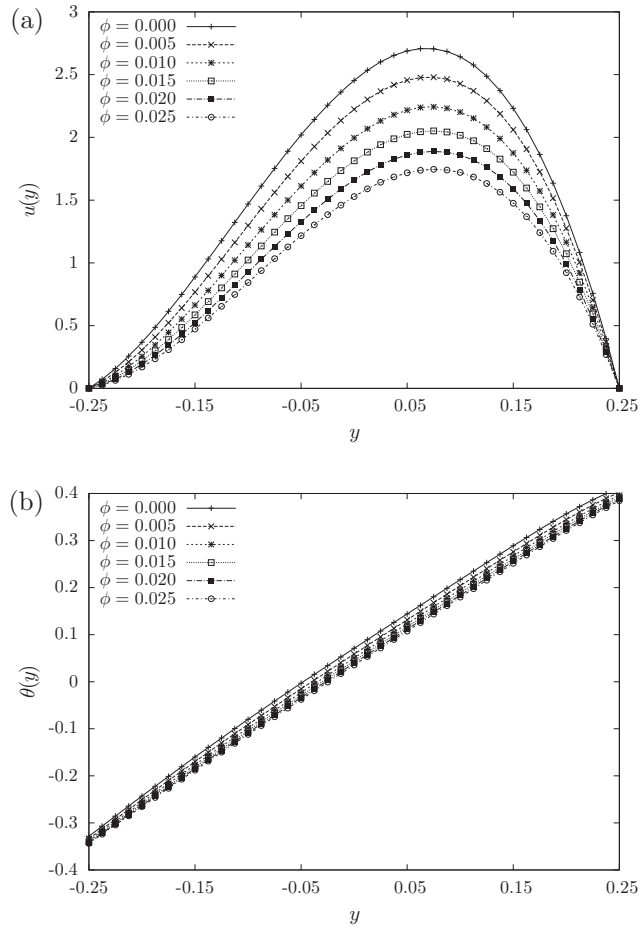

Figure 8 (a) Velocity profile and (b) temperature profile of Al_2O_3–water nanoliquid for different ϕ with $Br = 0.01, GR = 600$ and $Bi_1 = Bi_2 = 10$.

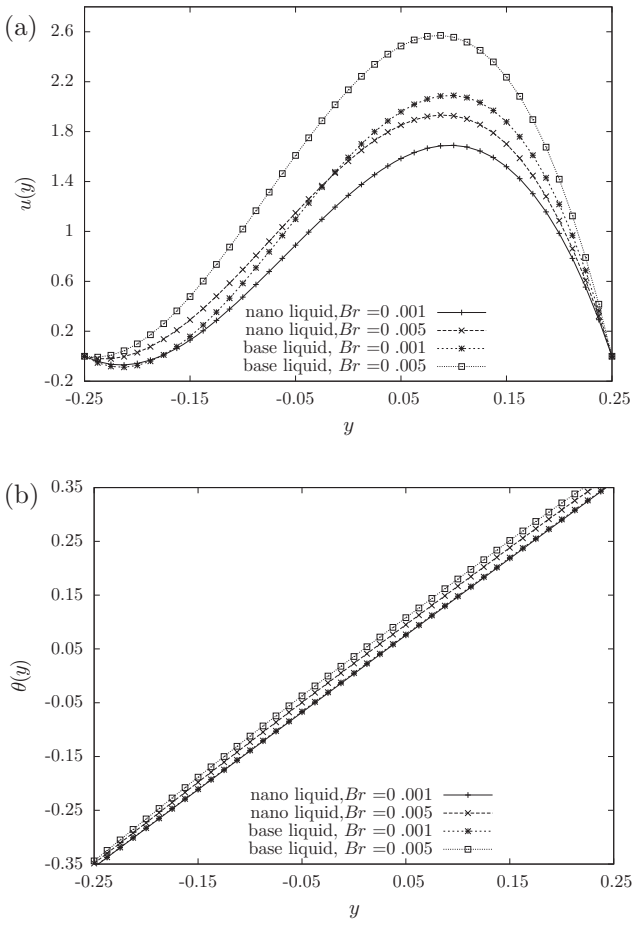

Figure 9 (a) Velocity profile and (b) temperature profile of Al_2O_3–water nanoliquid and base liquid for different Br with $GR = 600, \phi = 0.02$ and $Bi_1 = Bi_2 = 10$.

profile of Fig. 6, where with high value of Brinkman number $Br = 1.0$, the dimensionless velocity as well as dimensionless temperature of TiO_2–water is highest, followed by Al_2O_3–water and CuO–water.

Fig. 7 shows the temperature profiles and velocity profiles of nanoliquid (using Al_2O_3–water with $\phi = 0.02$) and base liquid with the purpose of looking into the effects of the gap between the values of Brinkman number Br and mixed convection parameter GR with Biot numbers $Bi_1 = Bi_2 = 10$ and nanoparticle volume fraction $\phi = 0.02$. Fig. 7(a) represents low value of GR and high value of Br, meanwhile Fig. 7(b) is otherwise. Looking into the temperature profiles, changes are not significant in Fig. 7(b) because viscous dissipation effect is reduced for the nanoliquids and base liquid for low Br. Therefore, viscous effect does not give a significant effect in determining the temperature distribution within the liquids. However, higher value of Br as in the temperature profile of Fig. 7(a) resulted in the importance of viscous effects in determining the temperature profile. Moreover, greater velocity gradient is produced with a larger value of GR, resulting in a greater viscous dissipation. This can clearly be seen in the temperature profile of Fig. 7(a), where the dimensionless temperature for $GR = 30$ is higher than $GR = 15$. Meanwhile, with low value of GR in Fig. 7(a), the velocity distribution is uniform for both the nanoliquid and base liquid. However, with higher values of GR as in the velocity profile of Fig. 7(b), the velocity distribution becomes less uniform with the maximum velocity approaches the hotter wall. When GR is greater than 300 (High value of GR), a reflux is formed, which resulted to the reversal of the velocity. This therefore leads to the occurrence of flow reversal at the colder wall.

In Fig. 8, the effects of increasing the nanoparticles concentration ϕ could be observed in the velocity profile Fig. 8(a) and the temperature profile Fig. 8(b), in which both profiles decrease with the increase in nanoparticle concentration. Looking into the temperature profile, the changes in the dimensionless temperature are less significant and heading towards a linear line as the value of ϕ increases. Meanwhile, in the velocity profile, the maximum value of the velocity occurs at the warmer part of the channel.

The dimensionless velocity and dimensionless temperature distributions, with a constant mixed convection parameter $GR = 600$, volume fractions of nanoparticles $\phi = 0.02$ and the Brinkman numbers $Br = 0.001$ and $Br = 0.005$ are shown in Fig. 9. It can be observed on the velocity profile that in comparison with base liquid, both values of the nanoliquids are lower and more uniformly distributed. The reason being is that the equivalent thermal expansion coefficient of base liquid is higher than nanoliquids. This condition leads to the reduction in the dimensionless velocity as the buoyancy force acting on

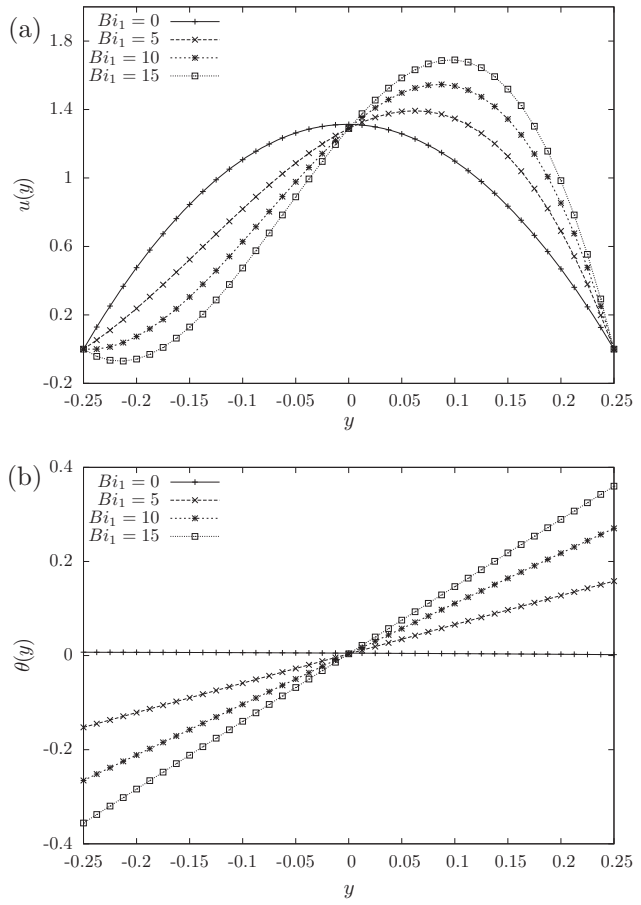

Figure 10 (a) Velocity profile and (b) temperature profile of Al_2O_3–water nanoliquids for different Bi_1 with $GR = 300$, $\phi = 0.02$, $Br = 0.001$ and $Bi_2 = 10$.

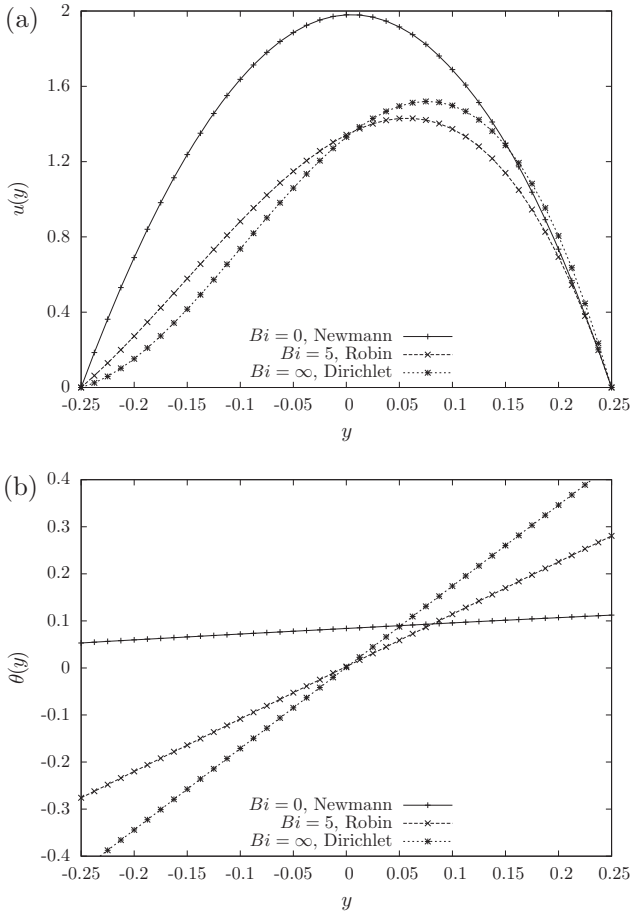

Figure 11 (a) Velocity profile and (b) temperature profile of Al_2O_3–water nanoliquids for three kinds of boundary conditions on temperature, $Bi = 0$ (Dirichlet), $Bi = 5$ (Robin) and $Bi \to \infty$ (Newmann) where $Bi_1 = Bi_2 = Bi, GR = 300, \phi = 0.02$ and $Br = 0.001$.

base liquid is also higher than that acting on nanoliquids. Furthermore, the velocity distribution is also more uniform, due to the value of viscosity and density of nanoliquids are greater than base liquid. Looking into the effect of viscous dissipation, as expected, the dimensionless temperature distribution is directly effected by the dimensionless velocity distribution. In the velocity profile, the viscous dissipation effect is increased due to the lower viscosity of base liquid, which resulted in the velocity gradient of base liquid is higher than nanoliquids. Besides that, heat is more readily transferred as the thermal conductivity coefficient of base liquid is lower than that of nanoliquids. Therefore, as can be observed in the temperature profile of Fig. 9(b), the dimensionless temperature of base liquid is higher than that of nanoliquids. However, this comparison is not that obvious with lower value of Brinkman number $Br = 0.001$.

Fig. 10 demonstrates the effect of Biot number Bi_1 on velocity and temperature profiles of Al_2O_3–water nanoliquid. It can be observed that both the velocity profile and temperature profile decrease with an increase in Bi_1 from the colder wall towards the centre of the channel and increase with the increase in Bi_1 from the centre of the channel towards the warmer wall. Biot numbers are the ratio of the hot liquid side convection resistance on a surface. Biot numbers are directly proportional to the heat transfer coefficients associated with the hot liquid, for fixed cold liquid properties. The thermal resistance on the hot liquid side is inversely proportional to the heat transfer coefficients. Thus, the hot liquid side convection resistance decreases and consequently, the surface temperature increases as Biot number Bi_1 increases. This result is also similar for the case of Biot number Bi_2 as well as for CuO–water and TiO_2–water nanoliquids.

Fig. 11 shows the influence of three different cases of boundary conditions on temperature, $Bi = 0$ (Dirichlet), $Bi = 10$ (Robin) and $Bi \to \infty$ (Newmann) on the velocity and temperature profiles. Looking into the velocity profile of Fig. 11(a), from the colder wall towards the centre of the channel, the velocity increases significantly for all the three cases of boundary conditions with $Bi = 0$ having the most rapid increase, followed by $Bi = 10$ and $Bi \to \infty$. When $Bi = 0$, the flow is symmetrical, but for the case of $Bi = 10$ and $Bi \to \infty$, the maximum velocity moves towards the hotter wall. Meanwhile, looking into the temperature profile of Fig. 11(b), when $Bi = 0$, the increase in temperature is less severe. However, the temperature increases more rapidly near the boundary for the case of $Bi = 10$ and most rapid when $Bi \to \infty$. The wall temperature increases with the increase in Biot numbers. It is expected that as Biot number goes to ∞, the convective boundary conditions will become the prescribed wall temperature

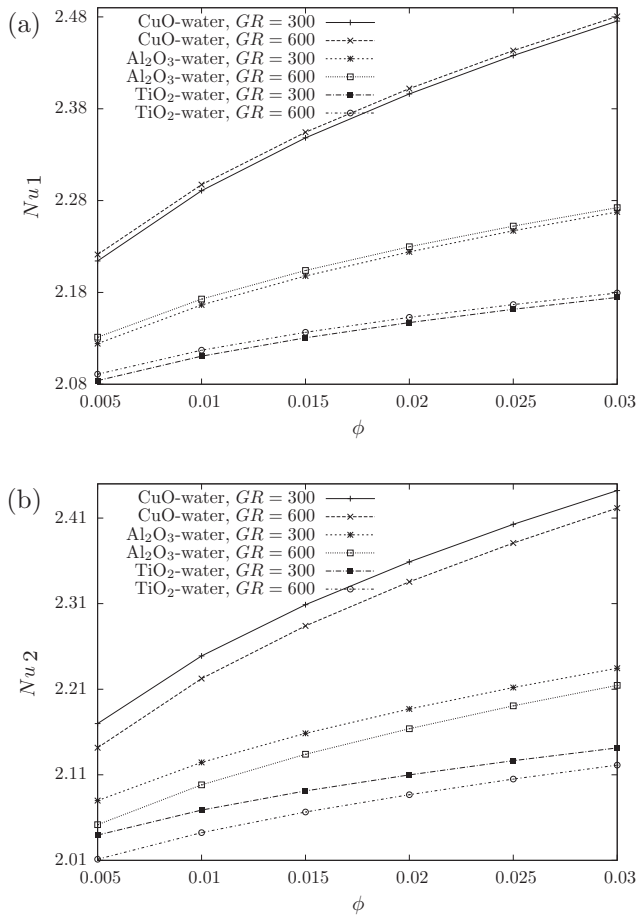

Figure 12 Variation of Nusselt number, (a) Nu_1 and (b) Nu_2 with variation in the value of GR with $Br = 0.001, Bi_1 = Bi_2 = 10$.

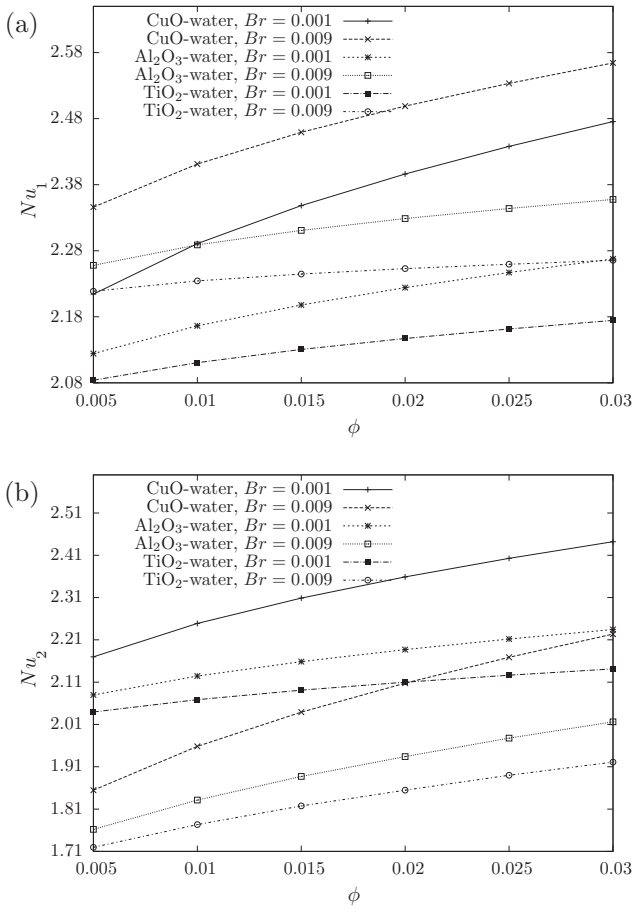

Figure 13 Variation of Nusselt number, (a) Nu_1 and (b) Nu_2 with variation in the value of Br with $Gr = 300, Bi_1 = Bi_2 = 10$.

case. We can notice that on the smaller domain of Dirichlet condition, the result would be unrealistic because the region of change reaches the boundary. Meanwhile, the Robin condition is more superior to the Newmann condition. The result obtained supports the research done by Novy et al. [23] Bixler [6] where it was concluded that the most accurate condition is the mixed condition (Robin condition), followed by the traction and free surface inclination boundary condition (Newman condition). The least satisfactory result is the Dirichlet boundary condition.

3.2. Heat transfer evaluation

To maximise the heat transfer efficiency with a smooth flow, the viscosity, the concentration of nanoparticles as well as the mixed convection parameter should be considered as important physical properties of a nanoliquids. Figs. 12–16 represent the figures involving Nusselt numbers (Nu_1 and Nu_2) of the water-based nanoliquids at various values of Br, GR, Bi_1 and Bi_2. The results are in good agreement with what was obtained by Majdi and Abed [21], where the Nusselt numbers increase with the increase in the value of nanoparticle volume fraction ϕ. It is observed that adding a low volume fraction of nanoparticles to the base liquid leads to significant increase in Nusselt number. Nanoliquids has higher mass concentration compared to the base liquid. Thus, the molecules of nanoliquids have higher momentum. This momentum carries and transfers thermal energy more efficiently at greater distance within the liquid before releasing the thermal energy in colder regions of the liquid.

Nusselt number Nu represents the heat transfer rate with Nu_1 referring to the colder wall and Nu_2 referring to the warmer wall. When $Nu_2 > 0$, heat-transfer direction at the hot wall is from the channel wall to the nanoliquid and when $Nu_2 < 0$, heat-transfer direction at the hot wall is from the nanoliquid to the channel wall. Similarly, When $Nu_1 > 0$, heat-transfer direction at the cold wall is from the nanoliquid to the wall and when $Nu_1 < 0$, heat-transfer direction at the cold wall is from the wall to the nanoliquid.

It is seen in Fig. 12 that the CuO–water nanoliquid possess a higher Nusselt number, on both the left wall Nu_1 in Fig. 12(a) and right wall Nu_2 in Fig. 12(b). This is followed by Al_2O_3–water and $Ti0_2$–water. The liquid velocity plays significant role on heat transfer, as the liquids move through the channel and CuO–water having the highest average velocity, due to lower density than base liquid. It can also be observed that the increase in mixed convection parameter GR gives a slight increase on all the three water-based nanoliquids for Nusselt number on the cold wall Nu_1. This is due to the minimal temperature difference between the cold wall and the nanoliquids and, consequently, the rate of heat transfer at the cold wall just have a slight increase. On the other hand, a significant decrease

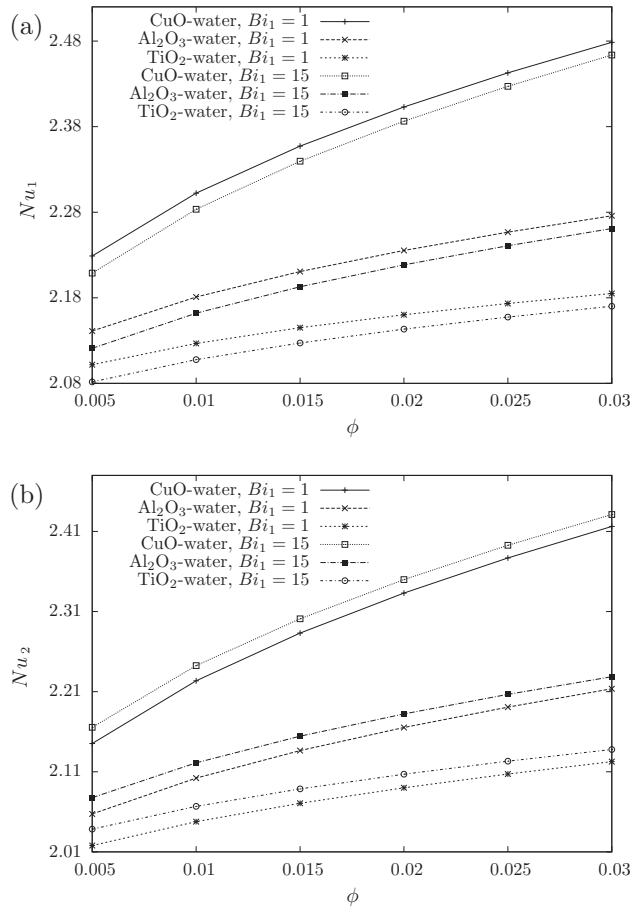

Figure 14 Variation of Nusselt number, (a) Nu_1 and (b) Nu_2 with variation in the value of Bi_1 with $Gr = 300$, $Br = 0.001$, $Bi_2 = 10$.

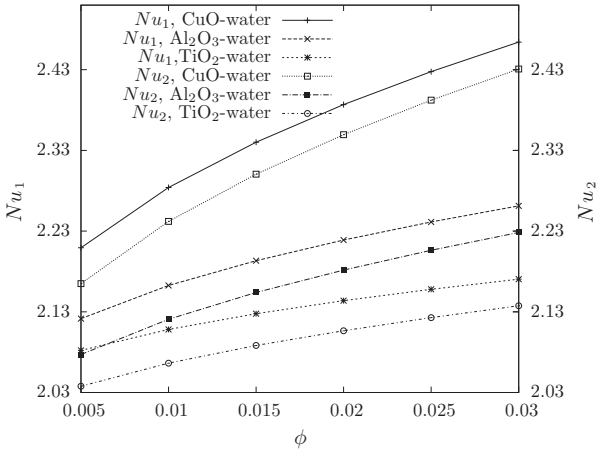

Figure 15 Variation of Nusselt numbers Nu_1 and Nu_2 of CuO–water, Al_2O_3–water and $Ti0_2$–water nanoliquids with $Gr = 300$, $Br = 0.001$, $Bi_1 = Bi_2 = 10$.

on Nusselt number at the warmer wall Nu_2 can be seen for all the three water-based nanoliquids with the increase in GR.

The Brinkman number is an important parameter governing the heat transfer and liquid flow of a vertical channel.

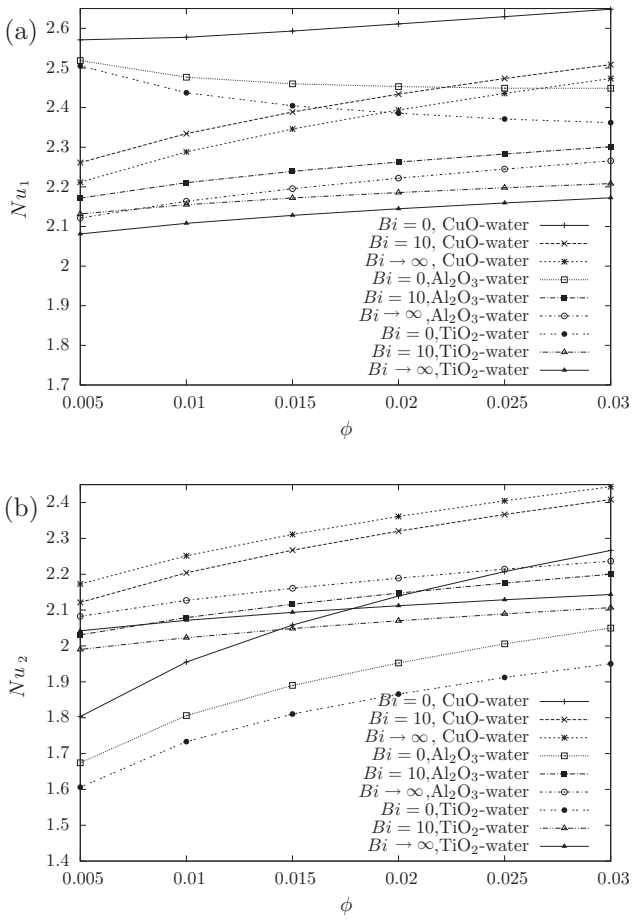

Figure 16 Variation of Nusselt numbers (a) Nu_1 and (b) Nu_2 of CuO–water, Al_2O_3–water and $Ti0_2$–water nanoliquids with three kinds of boundary conditions on temperature, $Bi = 0$ (Dirichlet), $Bi = 5$ (Robin) and $Bi \to \infty$ (Newmann) where $Bi_1 = Bi_2 = Bi$, $Br = 0.001$ and $GR = 300$.

The effects of viscous dissipation in a liquid flow and heat transfer are best described by the use of the Brinkman number. With the increase in Brinkman number, viscous dissipation increases, which leads to the increase in temperature. Fig. 13 aims at finding out the influence of the viscous dissipation effects on the temperature profile, and consequently, the Nusselt number. The figure shows that, unlike mixed convection parameter GR in Fig. 12 and Biot number Bi_1 in Fig. 14, Brinkman number in Fig. 13 gives a greater impact on the value of Nusselt numbers as ϕ increases. In Fig. 13(a), with the increase in Brinkman number, the liquid temperature will increase due to the increase in viscous dissipation. This will lead to the increase in the liquid and the cold wall temperature gradient and, consequently, Nu_1 increases. Meanwhile, the value of Nu_2 decreases with the increase in Br for all the three water-based nanoliquids.

Another result that is obvious in Figs. 12–16 is that the nanoliquids with CuO nanoparticle show higher enhancement in its Nusselt number, comparing to Al_2O_3 and TiO_2 nanoparticles. The reason being (as in Table 3) is due to the higher thermal conductivity of CuO–water nanoliquids with respect to Al_2O_3 and TiO_2 nanoliquids. Besides, as discussed in Seyf and Feizbakhshi [30], rapid alignment of Al_2O_3 and TiO_2

nanoliquids leads to less contact between the nanoparticles of Al_2O_3 and TiO_2 respectively and this consequently lowers heat transfer coefficient of the nanoliquids. Such difference in Nusselt number is due to difference between particle shapes, morphology, or surface treatment of CuO, Al_2O_3 and TiO_2 particles. Hence, CuO nanoparticle is clearly more efficient than Al_2O_3 and TiO_2 nanoparticles in increasing the Nusselt number of this study.

Figs. 16(a) and (b) represent the variation of Nusselt numbers, Nu_1 and Nu_2 respectively of CuO–water, Al_2O_3–water and TiO_2–water nanoliquids with three kinds of boundary conditions on temperature $Bi = 0$ (Dirichlet), $Bi = 10$ (Robin) and $Bi \to \infty$ (Newmann). Observing Fig. 16(a), it can be seen that as nanoparticle volume fraction ϕ increases, the rate of heat transfer reduces with higher values of Biot numbers for the three different types of water-based nanoliquids. This is resulted from the cooling effect of Biot numbers, which leads to the temperature difference between the liquid and the cold wall of the channel to decrease and therefore Nu_1 decreases. On the other hand, as in Fig. 16(b), increasing Biot numbers increases Nu_2 values for all the three water-based nanoliquids because as Bi increases, the thermal resistance of the hotter wall decreases and convective heat transfer to the liquid on the hotter wall increases. Among the three kinds of water-based nanoliquids, the effect of increasing ϕ is more profound in CuO–water nanoliquids. This is because the rate of heat transfer is higher in CuO–water nanoliquids than in Al_2O_3–water and TiO_2–water nanoliquids. Hence, a more effective improvement in the heat transfer performance is obtained.

4. Conclusion

In this work, fully-developed mixed convection heat transfer of CuO–water, Al_2O_3–water and TiO_2–water nanoliquids in a vertical channel by considering Dirichlet, Neumann and Robin boundary conditions has been studied. The dimensionless forms of the governing equations are solved using Runge−Kutta method with shooting technique. The major findings are as follows:

1. Reflow phenomenon occurs with sufficiently large value of mixed convection parameter, combined with a low value of Brinkman number.
2. The presence of nanoparticles in the base liquid causes a noticeable decrease in the velocity and the temperature profile and reflow occur with higher value of nanoparticle volume fraction.
3. Viscosity gives a greater impact than buoyancy and Biot numbers on the heat transfer rate as nanoparticle volume fraction increases.
4. Heat transfer rate at the cold wall and the hot wall increases with the increase in nanoparticle volume fraction.
5. The Robin boundary condition gives a more satisfactory and realistic result, in comparison with the Dirichlet condition and Newmann condition.

Acknowledgment

This study is supported by the research Grant FRGS/1/2014/SG04/04/UKM/01/1.

References

[1] M.H. Abolbashari, N. Freidoonimehr, F. Nazari, M.M. Rashidi, Analytical modeling of entropy generation for Casson nano-fluid flow induced by a stretching surface, Adv. Powder Technol. 26 (2) (2015) 542–5521.
[2] W. Aung, G. Worku, Theory of fully developed, combined convection including flow reversal, J. Heat Transfer 108 (2) (1986) 485–488.
[3] W.H. Azmi, K.V. Sharma, R. Mamat, A.B.S. Alias, I.I. Misnon, Correlations for thermal conductivity and viscosity of water based nanofluids, IOP Conf. Ser.: Mater. Sci. Eng. 36 (1) (2012) 12–29.
[4] A. Barletta, Laminar mixed convection with viscous dissipation in a vertical channel, Int. J. Heat Mass Transfer 41 (22) (1998) 3501–3513.
[5] A. Barletta, E. Zanchini, On the choice of the reference temperature for fully-developed mixed convection in a vertical channel, Int. J. Heat Mass Transfer 42 (16) (1999) 3169–3181.
[6] N. Bixler, Stability of a coating flow, Diss. Abst. Int. B: Sci. Eng. 43 (11) (1983).
[7] J. Buongiorno, Convective transport in nanofluids, J. Heat Transfer 128 (3) (2006) 240–250.
[8] K. Chao, B. Chen, C. Liu, Heat transfer and entropy generation in fully-developed mixed convection nanofluid flow in vertical channel, Int. J. Heat Mass Transfer 79 (2014) 750–758.
[9] C. Cheng, H. Kou, W. Huang, Flow reversal and heat transfer of fully developed mixed convection in vertical channels, J. Thermophys. Heat Transfer 4 (3) (1990) 375–383.
[10] S. Choi, J. Eastman, Enhancing thermal conductivity of fluids with nanoparticles, ASME-Int. Mech. Eng. Congress Exposition 231 (1995) 99–106.
[11] S. Das, R. Jana, O. Makinde, Mixed convective magnetohydrodynamic flow in a vertical channel filled with nanofluids, Int. J. Eng. Sci. Technol. 18 (2) (2015) 244–255.
[12] M. Fakour, A. Vahabzadeh, D. Ganji, Scrutiny of mixed convection flow of a nanofluid in a vertical channel, Case Stud. Therm. Eng. 4 (2014) 15–23.
[13] U. Farooq, T. Hayat, A. Alsaedi, S. Liao, Heat and mass transfer of two-layer flows of third-grade nano-fluids in a vertical channel, Appl. Math. Comput. 242 (2014) 528–540.
[14] N. Freidoonimehr, M.M. Rashidi, S. Mahmud, Unsteady MHD free convective flow past a permeable stretching vertical surface in a nano-fluid, Int. J. Therm. Sci. 87 (2015) 136–145.
[15] T. Grosan, I. Pop, Thermal radiation effect on fully developed mixed convection flow in a vertical channel, Tech. Mech. 27 (1) (2007) 37–47.
[16] M. Hajipour, A. Dehkordi, Analysis of nanofluid heat transfer in parallel-plate vertical channels partially filled with porous medium, Int. J. Therm. Sci. 55 (2012) 103–113.
[17] F. Incropera, Buoyancy effects in double-diffusive mixed convection flows, Proc. Eighth Int. Conf. 1 (1986) 121–130.
[18] V. Javeri, Simultaneous development of the laminar velocity and temperature fields in a circular duct for the temperature boundary condition of the third kind, Int. J. Heat Mass Transfer 19 (8) (1976) 943–949.
[19] K. Khanafer, K. Vafai, M. Lightstone, Buoyancy-driven heat transfer enhancement in a two-dimensional enclosure utilizing nanofluids, Int. J. Heat Mass Transfer 46 (19) (2003) 3639–3653.
[20] O. Mahian, I. Pop, A. Sahin, H. Oztop, S. Wongwises, Irreversibility analysis of a vertical annulus using TiO_2/water nanofluid with mhd flow effects, Int. J. Heat Mass Transfer 64 (2013) 671–679.
[21] H. Majdi, A. Abed, Effect of nanofluids on the performance of corrugated channel within out-of-phase arrangement, Int. J. Sci. Technol. Res. 3 (1) (2014) 220–229.

[22] A. Malvandi, D. Ganji, Effects of nanoparticle migration on hydromagnetic mixed convection of alumina/water nanofluid in vertical channels with asymmetric heating, Physica E: Low-dimensional Syst. Nanostruct. 66 (2015) 181–196.
[23] R. Novy, H. Davis, L. Scriven, A comparison of synthetic boundary conditions for continuous-flow systems, Chem. Eng. Sci. 46 (1) (1991) 57–68.
[24] T. Papanastasiou, N. Malamataris, K. Ellwood, A new outflow boundary condition, Int. J. Numer. Methods Fluids 14 (1992) 587–608.
[25] H.E. Patel, T. Sundararajan, S.K. Das, An experimental investigation into the thermal conductivity enhancement in oxide and metallic nanofluids, J. Nanoparticle Res. 12 (3) (2010) 1015–1031.
[26] I. Pop, T. Grosan, R. Cornelia, Effect of heat generated by an exothermic reaction on the fully developed mixed convection flow in a vertical channel, Commun. Nonlinear Sci. Numer. Simul. 15 (3) (2010) 471–474.
[27] M.M. Rashidi, N. Freidoonimehr, E. Momoniat, B. Rostami, Study of nonlinear MHD tribological squeeze film at generalized magnetic reynolds numbers using DTM, PloS One 10 (8) (2015) e0135004.
[28] M.M. Rashidi, S. Shohel, N. Freidoonimehr, B. Rostami, Analysis of entropy generation in an MHD flow over a rotating porous disk with variable physical properties, Int. J. Exergy 16 (4) (2015) 481–503.
[29] H. Saleh, I. Hashim, S. Basriati, Flow reversal of fully developed mixed convection in a vertical channel with chemical reaction, Int. J. Chem. Eng. 2013 (2013) 1–4.
[30] H. Seyf, M. Feizbakhshi, Computational analysis of nanofluid effects on convective heat transfer enhancement of micro-pin-fin heat sinks, Int. J. Therm. Sci. 58 (2012) 168–179.
[31] L. Tao, On combined free and forced convection in channels, J. Heat Transfer 82 (3) (1960) 233–238.
[32] A. Utomo, H. Poth, P. Robbins, A. Pacek, Experimental and theoretical studies of thermal conductivity, viscosity and heat transfer coefficient of titania and alumina nanofluids, Int. J. Heat Mass Transfer 55 (25) (2012) 7772–7781.
[33] H. Xu, T. Fan, I. Pop, Analysis of mixed convection flow of a nanofluid in a vertical channel with the buongiorno mathematical model, Int. Commun. Heat Mass Transfer 44 (2013) 15–22.
[34] H. Xu, I. Pop, Fully developed mixed convection flow in a vertical channel filled with nanofluids, Int. Commun. Heat Mass Transfer 39 (8) (2012) 1086–1092.
[35] E. Zanchini, Effect of viscous dissipation on mixed convection in a vertical channel with boundary conditions of the third kind, Int. J. Heat Mass Transfer 41 (23) (1998) 3949–3959.